Neutron Stars as a Probe of the Equation of State

J. M. Lattimer
Stony Brook University, Stony Brook, NY 11733, USA

Neutron stars are the densest massive objects in the universe. They are ideal astrophysical laboratories to test theories of dense matter physics and provide connections among nuclear physics, particle physics and astrophysics. Recent observations, including studies of binary pulsars, thermal emission from both isolated and accreting neutron stars, and glitches from pulsars provide information about neutron star masses, radii, temperatures, ages and internal compositions. Of particular recent interest are new estimates of masses in radio binary pulsars and a proposition that the relativistic binary pulsar PSR J0737-3039 could give a moment of inertia measurement.

1. GLOBAL ASPECTS OF NEUTRON STARS

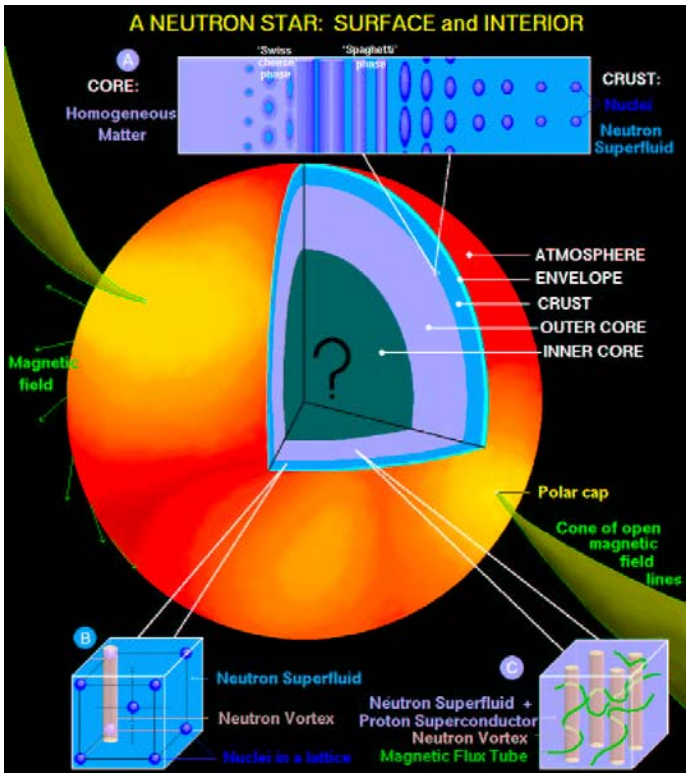

Figure 1: Internal structure of a neutron star, courtesy Dany Page.

Neutron stars can be broadly categorized as being normal or self-bound. Normal neutron stars are largely composed of nucleonic matter and have surfaces where both the pressure and energy density vanish. Normal stars may have *exotic* matter, such as hyperons, Bose condensates (pions or kaons) and/or nearly free quark matter in their interiors. Self-bound stars, on the other hand, have surfaces at which the pressure vanishes but the energy density remains finite. The best-known example of a self-bound star is a star composed completely of strange quark matter. Although there exists no convincing observational evidence that strange quark matter stars exist, they remain a tantalizing possibility if the ultimate ground state of matter is strange quark matter, not nucleonic matter.

The internal structure of a normal neutron star is depicted in Figure 1. The star can be viewed as having 5 regions.

- The atmosphere shapes the thermal optical, ultraviolet and x-ray spectrum.
- The envelope, whose composition determines its relative effectiveness as an insulating layer, has densities ranging below 1 g cm^{-3}.
- In the density range up to about 10^{14} g cm^{-3}, the crust is chiefly populated with nuclei and electrons. Above the neutron drip density ($4 \cdot 10^{11}$ g cm^{-3}) a sea of (likely superfluid) neutrons accompanies the nuclei and becomes more abundant at higher densities. A popular model for glitches involves weak coupling between normal and superfluid matter within the crust.
- The outer core consists of nucleons, electrons and muons. Protons in the outer core may be superconducting.
- Depending upon the stellar mass and the relative stiffness of matter, an inner core with exotic matter may exist.

The global structure of neutron stars is conveniently displayed using mass- radius diagrams (Figure 2) which highlight the variations allowed by uncertainties in the underlying dense matter equation of state (EOS, *i.e.*, $P(\rho)$, where P is the pressure and ρ is the energy density of matter). These structures are computed utilizing the Tolman-Oppenheimer-Volkoff relativistic structure equations.

The upper left and lower right regions of Figure 2 can be excluded from consideration on the basis of general relativity and other physical constraints. These limits include

- The Schwarzschild constraint, $R > 2GM/c^2$, that the star's surface does not lie within its event horizon.

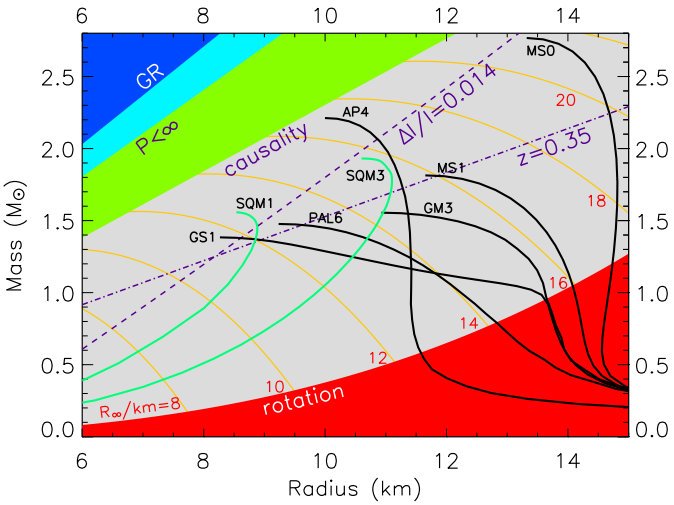

Figure 2: Mass-radius diagram. The blue region 'GR' is excluded by general relativity, the light blue region by finite pressures, and the green region by causality. Solid black curves depict normal neutron stars; solid green curves show strange quark matter stars. EOS labels are defined in [1]. Orange contours show fixed values of R_∞. The dashed curve shows a radius limit from glitches, the dash-dot curve shows the redshift $z = 0.35$, and the red region is excluded by the most rapidly rotating pulsar ($P = 1.6$ ms).

- The condition that the central pressure remains finite, $P_c < \infty$, or $R > (9/4)GM/c^2$.
- The condition that the sound speed within the star remain less than the speed of light, $\partial P/\partial\rho \leq c^2$. This results in, approximately, $R > 3.01GM/c^2$ [2, 3].
- The condition that the most rapidly rotating neutron star rotate with a frequency ν less than the mass-shedding limit where the surface rotates with the Keplerian frequency. For a rigid sphere $2\pi\nu = \sqrt{GM/R^3}$. A rapidly spinning star is deformed, and for a neutron star, general relativistic effects are substantial. Nevertheless, a relatively EOS-independent limit can be deduced[5]:

$$\nu \leq 1045 \pm 30 \sqrt{\frac{M}{\mathrm{M}_\odot}} \left(\frac{10\ \mathrm{km}}{R_0}\right)^{3/2} \ \mathrm{Hz}. \qquad (1)$$

Other inferred limits have come from pulsar glitches. Several pulsars exhibit stochastic breaks in their otherwise regular pulsing frequencies. A glitch is a sudden increase in pulsar spin frequency (by a part in 10^7 or so) which relaxes over a period of weeks toward the original spin frequency. From the cumulative number and magnitudes ofthe glitches in the case of the Vela pulsar over a period of 30 years, it can be inferred that at least 1.4% of the total moment of inertia of the star is contained in the region responsible for glitches[4]. Presumably this region is the neutron star crust. It can be demonstrated that the fractional moment of inertia $\Delta I/I$ of the crust is approximately proportional to $P_t R^4/M^2$ where P_t is the pressure of matter at the core-crust interface. Although the value of P_t is uncertain by about a factor of 3 or 4, the largest possible value of P_t, together with the above lower limit to $\Delta I/I$, permits a lower limit to R for a given M to be established. This limit is shown in Figure 2.

Other constraints could be established from the redshifts of spectral lines or from radiation radii

$$R_\infty = R/\sqrt{1 - 2GM/(Rc^2)} \qquad (2)$$

determined from thermal emission from neutron stars. Recently, wide lines were observed in the x-ray burst source EXO 0748-676. A tentative identification with heavy element lines has resulted in the estimate of $z = (1 - 2GM/c^2)^{-1/2} - 1 \simeq 0.35$ for this source. Unfortunately, no reliable estimates for the radiation radius R_∞ have been possible from observed thermally-emitting neutron stars. Problems include uncertainties in the neutron star atmosphere, the strength and structure of surface magnetic fields, and distances. Inferred values of R_∞ are directly proportional to the distance.

2. CHARACTERISTICS OF THE EQUATION OF STATE

Normal matter EOS's generally satisfy the polytropic relation $P \propto n^2$ in the vicinity of the nuclear saturation density, $n_s \simeq 2.7{\cdot}10^{14}$ g cm$^{-3} \simeq 0.16$ fm^{-3}. The EOS's used in Figure 2 and several additional examples are plotted in Figure 3. At large densities, each of these EOS's eventually softens, in some cases due to the appearance of exotic matter. In any event, the restriction of causality requires this behavior.

A Newtonian polytropic star with index N obeys the scaling

$$\begin{aligned} R &\propto K^{N/(3-N)} M^{(1-N)/(3-N)} \\ &\propto P_0^{N/(3-N)} n_0^{-(N+1)/(3-N)} M^{(1-N)/(3-N)} \end{aligned} \qquad (3)$$

where $K = P_0/n_0^{1+1/N}$ and the subscript 0 refers to a fiducial density. In the case $N = 1$ one has

$$R \propto P_0^{1/2} n_0^{-1} M^0 \qquad (4)$$

so that the radius is insensitive to the mass. Indeed, this behavior is apparent in Figure 2 for many EOS's for stars with masses in the range $0.5\ \mathrm{M}_\odot < M < 1.5\ \mathrm{M}_\odot$. The above relation also suggeststst that a radius measurement could give some information about

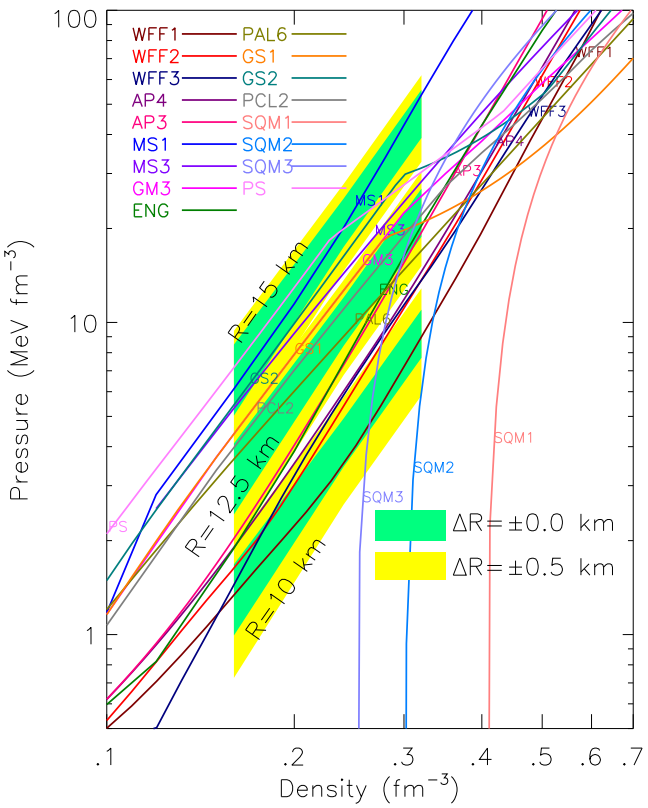

Figure 3: Pressure of various equations of state (see Ref. [1] for descriptions and references) as a function of baryon densities. Green and yellow shaded regions display hypothetical confidence bands for three radius measurements with the indicated uncertainties.

Table I Pressure-Radius Correlation Constant $C_M(n_0)$, dimensions km fm$^{3/4}$ MeV$^{-1/4}$

n_0/n_s	1 $M_\odot$	1.5 $M_\odot$
1.0	9.53 ± 0.32	9.30 ± 0.60
1.5	7.14 ± 0.15	7.00 ± 0.31
2.0	5.82 ± 0.21	5.72 ± 0.25

P_0. Reference [1] has, in fact, found precisely that. They found the phenomenological relation

$$R_M = C_M(n_0) P_0(n_0)^{1/4} \tag{5}$$

where R_M is the radius of a star of mass M, $P_0(n_0$ is the pressure at the density n_0, and $C_M(n_0)$ is a constant fitted to a large number of EOS's (rms errors are typically less than 5% for $n_s < n_0 < 2n_s$).

It should also be noted from Figure 3 that there is a large uncertainty in P_0, about a factor of 6. This accounts for the estimated range of neutron star radii 9 km $< R <$ 16 km. This uncertainty in P_0 can be traced directly to the uncertainty in the so-called symmetry energy of nuclear matter. Near the nuclear saturation density n_s and for nearly symmetric cold matter (*i.e.*, $x \equiv n_p/(n_n + n_p) \simeq 1/2$ and $T = 0$) one can expand the energy per baryon of nucleonic matter:

$$\begin{aligned} E(n,x) &= -16 + \frac{K}{18}\left(1 - \frac{n}{n_s}\right)^2 + \frac{K'}{27}\left(1 - \frac{n}{n_s}\right)^3 \\ &+ E_{sym}(n)(1-2x)^2 \ldots . \end{aligned} \tag{6}$$

Here, K and K' are the incompressibility and skewness parameters, respectively, and E_{sym} is the symmetry energy function, approximately equivalent to the energy difference at a given density between symmetric and pure neutron matter. The symmetry energy parameter is defined as $S_v \equiv E_{sym}(n_s)$. Leptonic contributions $E_e = (3/4)\hbar c x (3\pi^2 n x^4)^{1/3}$ must be added to ensure charge neutrality. Matter in neutron stars is in beta equilibrium, *i.e.*,

$$\mu_e = \mu_n - \mu_p = -\partial E/\partial x, \tag{7}$$

so the the equilibrium proton fraction at n_s is

$$x_s \simeq (3\pi^2 n_s)^{-1} (4 S_v/\hbar c)^3 \simeq 0.04. \tag{8}$$

The pressure at n_s is

$$\begin{aligned} P(n_s, x_s) &= n_s(1-2x_s)[n_s S_v'(1-2x_s) + S_v x_s] \\ &\simeq n_s^2 S_v' , \end{aligned} \tag{9}$$

due the small value of x_s. Here $S_v' \equiv (dE_{sym}/dn)_{n_s}$. **Thus the pressure depends primarily upon S_v'.**

The equilibrium pressure at moderately larger densities similarly is insensitive to K and K' and controlled by dE_{sym}/dn. Experimental constraints to the compression modulus K, most importantly from analyses [6] of giant monopole resonances, give $K \cong 220$ MeV. The skewness parameter K' has been estimated to lie in the range 1780–2380 MeV [7]. Evaluating the pressure for $n = 1.5 n_s$,

$$\begin{aligned} P(1.5n_s) &= 2.25 n_s [K/18 - K'/216 \\ &+ n_s (1-2x)^2 (dE_{sym}/dn)_{1.5n_s}] , \end{aligned} \tag{10}$$

and it is noted that the contributions from K and K' largely cancel.

It is known that dE_{sym}/dn for $n < n_s$ is partially constrained by the nuclear surface energy[8, 9]. Nuclear binding energies yield a significant correlation between S_v and S_v', but cannot determine either with precision. It is hoped that experiments to measure the neutron skin thickness of Pb and other experiments using rare-isotope accelerators to probe neutron-rich heavy elements will become sufficiently precise to provide an independent, second, correlation that could break the existing degeneracy.

3. ANALYTIC SOLUTIONS OF EINSTEIN'S EQUATIONS

Some insight into the global structures of neutron stars can be obtained by investigating selected analytic solutions's to the Tolman-Oppenheimer-Volkoff

equation. With the constraint that the pressure and energy density both vanish at the surface R, only 3 analytic solutions are currently known. These are due to Tolman [10], Nariai [11], and Buchdahl [12]. An infinite set of analytic solutions are known for the case in which the energy density is not required to vanish at the surface (the self-bound case). Of the three former solutions, those due to Tolman and Buchdahl are especially interesting.

Tolman's solution has a simple density profile

$$\rho = \rho_c[1 - (r/R)^2] \tag{11}$$

leading to the radius-mass relation

$$R = \left(\frac{15M}{8\pi\rho_c}\right)^{1/3}. \tag{12}$$

Buchdahl's is the only analytic solution with an explicit EOS

$$\rho c^2 = \sqrt{PP_*} - 5P, \tag{13}$$

which in the low-density limit is just a polytrope with index N=1. In these equations, ρ_c is the central energy density and P_* is a constant reference pressure. Buchdahl's solution has the radius-mass relation

$$R = \sqrt{\frac{\pi c^4(1-\beta)^2}{2GP_*(1-2\beta)}}, \tag{14}$$

where $\beta = GM/Rc^2$. This relation can be used to justify the phenomenological relation Eq. 5. Differentiation of Eq. 14 leads to the exponent

$$\left.\frac{d\ln R}{d\ln P}\right|_{n_0,M} = \frac{1}{2}\frac{(1-10\sqrt{P/P_*})}{(1+2\sqrt{P/P_*})}\frac{(1-\beta)(1-2\beta)}{(1-3\beta+3\beta^2)}. \tag{15}$$

Note that Eq. 15 predicts an exponent 1/2 in the limit $\beta \to 0$ and $P_0 \to 0$. Finite values of β and P_0 reduce the exponent. If M and R are about 1.4 $M_\odot$ and 15 km, respectively, for example, $\beta \simeq 0.14$ and Eq. 14 gives $P_* = .5\pi/R^2 \approx 6.98\cdot 10^{-3}$ km^{-2} (in geometrized units where $G = c = 1$). At a fiducial density $n_0 = 1.5n_s$, equivalent in geometrized units to $n_0 = 2.02 \cdot 10^{-4}$ km^{-2}, Eq. 13 then implies $P_0/P_* \simeq 28.8$ and Eq. 15 yields an exponent of about 0.28.

It is also interesting to examine analytic solutions for self-bound stars. The simplest of these is that of the constant density fluid, for which

$$R = \left(\frac{3M}{4\pi\rho_c}\right)^{1/3}. \tag{16}$$

Strictly speaking, this solution is relatively nonphysical because it has an infinite sound speed. The simplest of the analytic self-bound cases with finite sound speeds is a solution recently found by Lake [13]. This solution has a radius-mass relation given by

$$4\pi\rho R^2 = \beta(2-2\beta)^{2/3}\frac{6-15\beta+5\beta(r/R)^2}{(2-5\beta+3\beta(r/R)^2)^{5/3}} \tag{17}$$

and a pressure profile given by

$$4\pi\frac{P}{c^2}R^2 = \frac{\beta}{2-5\beta+\beta(r/R)^2}\times \left[2 - \frac{(2-2\beta)^{2/3}(2-5\beta+5\beta(r/R)^2)}{(2-5\beta+3\beta(r/R)^2)^{2/3}}\right]. \tag{18}$$

This particular solution has the interesting property that the speed of sound c_s throughout the interior has a value $c_s^2 \approx 1/3$, which is approximately the case for strange quark matter stars. In the high-density limit, asymptotically free quark matter has $c_s^2 = 1/3$.

4. MAXIMUM DENSITY AND MASS

Assuming the EOS is known up to a fiducial energy density ρ_0, and assuming an upper limit $c_s^2 = 1$ for matter at higher densities, it can be shown [15] that the maximum neutron star mass satisfies

$$M_{max} \simeq 4.1\sqrt{\rho_s/\rho_0}\ \mathrm{M}_\odot \tag{19}$$

where ρ_s is the nuclear saturation density. Similarly, the radius of the maximum mass star satisfies

$$R_{max} \geq 3.01\frac{GM_{max}}{c^2}\ \mathrm{km}. \tag{20}$$

If such stars were incompressible, this would suggest that the central density ρ_c would have to be less than the value

$$\rho_{c,Inc} \leq \frac{3}{4\pi M_{max}^2}\left(\frac{c^2}{3.1G}\right)^3 \simeq 5.5\cdot 10^{15}(\mathrm{M}_\odot/M)^2\ \mathrm{g\ cm^{-3}}. \tag{21}$$

However, the constant density solution violates causality, and thus represents a severe underestimate to the limiting density. Interestingly the corresponding limit determined using the Tolman solution (Eq. 12) actually does bound all realistic EOS's [14]:

$$\rho_{c,T} = \frac{5}{2}\rho_{c,Inc} \leq 13.8\cdot 10^{15}(\mathrm{M}_\odot/M)^2\ \mathrm{g\ cm^{-3}}. \tag{22}$$

It is shown in Figure 4, which includes results from a large number of EOS's of various types, with and without exotic components.

One of the most exciting recent developments is the accumulation of significant mass information for neutron stars. Almost exclusively, this data comes from neutron stars in close binary systems (see Figure 5. The most accurately measured masses are from timing

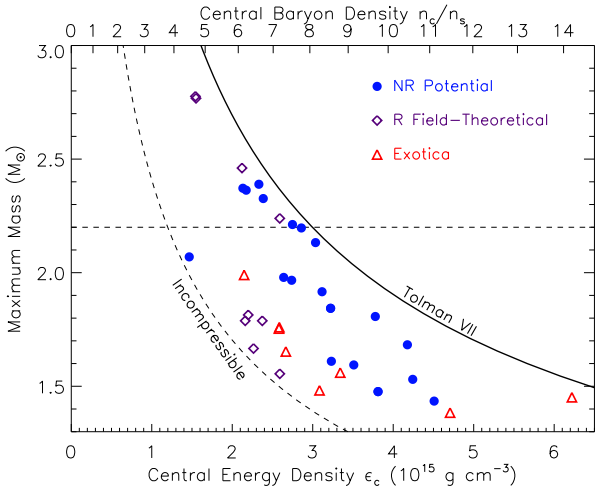

Figure 4: Central energy densities as a function of maximum masses for various equations of state. NR=non-relativistic, R=relativistic. For comparison, limiting central energy densities for the constant-density and the Tolman solutions are displayed. The upper scale for baryon density is a rough approximation since the precise conversion is EOS-dependent. The horizontal line at $M = 2.2$ M$_\odot$ is to guide the eye. From Ref. [14].

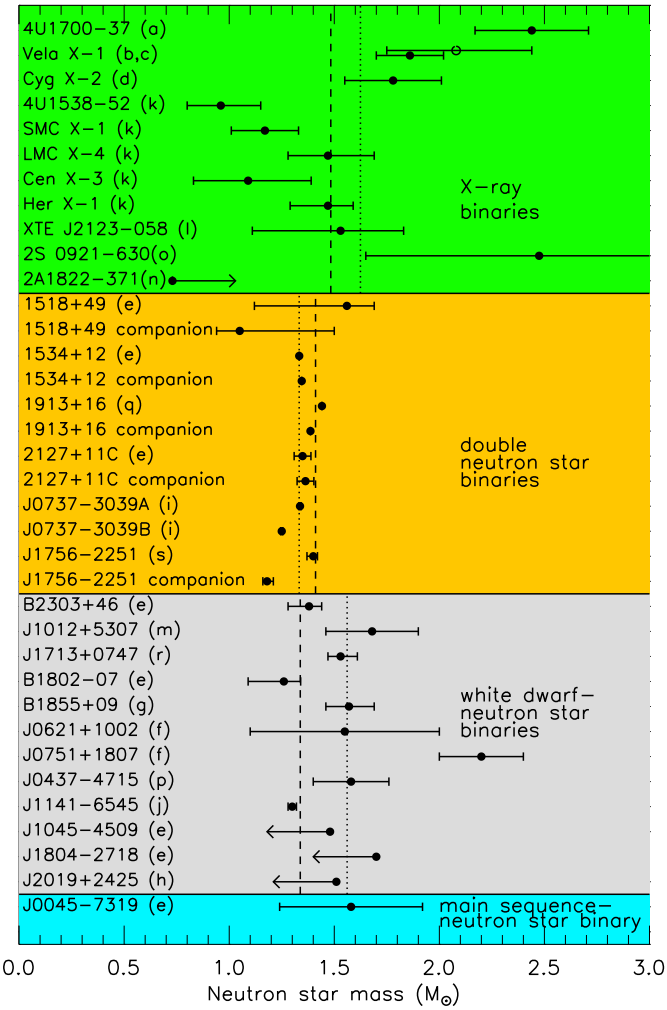

Figure 5: Measured and estimated masses of neutron stars in radio binary pulsars (gold, silver and blue regions) and in X-ray binaries (green). Letters following binary names indicate references which are provided in Ref. [14].

observations of the radio binary pulsars[16]. Ordinarily, observations of binary pulsars yield orbital sizes andperiods from Doppler phenomena, from which the total mass of the binary can be deduced. But the compact nature of these binaries permits, in some cases, detection of relativistic effects, such as Shapiro delay or orbit shrinkage due to emission of gravitational waves, which constrains the inclination angle and permits the mass ratios to be determined. A sufficiently well-observed system can have masses measured to impressive accuracy. The textbook case is the binary pulsar PSR B1913+16, in which the masses are 1.3867 ± 0.0002 and 1.4414 ± 0.0002 M$_\odot$[17].

It is interesting that radio binaries with white dwarf companions exhibit a broader range of neutron star masses than double neutron star binaries. Ref. [18] suggested that a rather narrow set of initial conditions are needed to form double neutron star binaries, including initial stellar masses that are nearly equal and are also in a restricted range. This leads to neutron star masses that therefore display only limited variations. These restrictions are relaxed for other neutron star binaries. As Figure 5 indicates, a few of the neutron stars in the white dwarf binaries may contain neutron stars considerably larger than the canonical 1.4 M$_\odot$ value, including the case of PSR J0751+1807 in which the 1σ error range is 2–2.4 M$_\odot$, and 1.4 M$_\odot$ is about a 4σ excursion. Indeed, the mean observed masses in white dwarf binaries exceeds that of the double neutron star binaries by about 0.25 M$_\odot$, although the 2σ error ranges for all but one of these systems extends below 1.45 M$_\odot$.

Masses can also be estimated for another handful of binaries which contain an accreting neutron star emitting X-rays (see Figure 5). Some of these systems are characterized by relative large masses, but their estimated errors are also large. The system of Vela X-1 is noteworthy because the lower mass limit (1.6–1.7 M$_\odot$) is constrained by geometry[19]. One should note that it is not definite that all of the X-ray sources in Figure 5 contain neutron stars. The source 4U 1700-37 might be a black hole, due to lack of oscillations in its X-ray spectrum[20]. Another high-mass object, 2S 0921-630[21] could either be a high-mass neutron star or a low-mass black hole. These two objects could play a role in determining the neutron star maximum mass and black hole minimum mass division.

5. MOMENTS OF INERTIA

We have already discussed how glitches can be used to set constraints on the crustal fraction of the moment of inertia. However, the possibility exists in sufficiently relativistic binaries to use spin-orbit coupling to determine the moment of inertia of the more rapidly spinning neutron star. The recently discovered [22] relativistic binary pulsar PSR J0737-3039 could become the first in which a neutron star moment of inertia is measured.

There are two kinds of spin-coupled precession effects in a binary system of compact stars: spin-orbit and spin-spin couplings (for a comprehensive discussion, see Refs. [23, 24]). Spin-orbit coupling leads to a precession of the angular momentum vector $\vec{L}$ of the orbital plane around the direction of the total angular momentum $\vec{J}$ of the system. This is sometimes called geodetic precession, and is related to the Thomas precession of atomic physics. Since the total angular momentum $\vec{J} = \vec{L} + \vec{S}_A + \vec{S}_B$ is conserved (at this order), there are compensating precessions of the spins $\vec{S}_A$ and $\vec{S}_B$ of the two stars. Since the orbital angular momentum dominates the spin angular momenta in binaries, the geodetic precession amplitude is very small while the associated spin precession amplitudes are substantial. In addition to geodetic precession, spin-orbit coupling also manifests itself in apsidal motion (advance of the periastron). Spin-spin coupling is generally negligible in binary systems because $|\vec{L}| >> |\vec{S}_A|, |\vec{S}_B|$.

According to [23], the spin and orbital angular momenta evolve according to

$$\begin{aligned} \dot{\vec{S}}_i &= \frac{G(4M_i + 3M_{-i})}{2M_i a^3 c^2 (1-e^2)^{3/2}} \vec{L} \times \vec{S}_i, \\ \dot{\vec{L}}^{SO} &= \sum_i \frac{G(4M_i + 3M_{-i})}{2M_i a^3 c^2 (1-e^2)^{3/2}} \left(\vec{S}_i - 3 \frac{\vec{L} \cdot \vec{S}_i}{|\vec{L}|^2} \vec{L} \right), \end{aligned} \quad (23)$$

where the superscript SO refers to the spin-coupling contribution only (there are also first- and second-order post-Newtonian terms, 1PN and 2PN, respectively, unrelated to the spins, that contribute to this order). Here a is the semimajor axis of the effective one-body orbital problem (sum of the semi-major axes of the two stellar orbits), e is the eccentricity, and M_i and M_{-i} refer to the masses of the two binary components (for $i = A, B$ we use $-i = B, A$). To this order, one may employ the Newtonian relation for the orbital angular momentum

$$|\vec{L}| = \frac{2\pi M_A M_B a^2 \sqrt{1-e^2}}{MP} = M_A M_B \sqrt{\frac{Ga(1-e^2)}{M}} \quad (24)$$

where P is the orbital period and $M = M_A + M_B$. Then, from Eq. 23, the spin precession periods are

$$P_{p,i} = \frac{2c^2 aPM(1-e^2)}{GM_{-i}(4M_i + 3M_{-i})}, \quad (25)$$

which are not identical for the two components unless they are of equal mass. The spin precession periods are independent of the spins, and in the case of PSR J0737-3039 are relatively short, being of order 75 years for each pulsar. If the spins are parallel to $\vec{L}$, there is no spin precession and the spin-orbit contribution to the advance of the periastron is in the sense opposite to the direction of motion. However, this does not appear to be the case for PSR J0737-3039.

The spin precession leads to two observable effects. First, as the spin axis change orientation in space, the pulsar beams will sweep through changing directions in space. In many cases, this will lead to the periodic appearance and disappearance of the pulsar beam from the Earth. Second, since total angular momentum is conserved (to this order), the orbital plane will change orientation. This will be observed as a periodic change in the inclination angle i with amplitude

$$\delta_i = \frac{|\vec{S_A}|}{|\vec{L}|} \sin\theta_A \simeq \frac{I_A M}{a^2 M_A M_B (1-e^2)^{1/2}} \frac{P}{P_A} \sin\theta_A, \quad (26)$$

where I_A is the moment of inertia of pulsar A. This in turn causes a periodic departure from the expected time-of-arrival of pulses from pulsar A with amplitude

$$\delta t_A = \frac{M_B}{M} \frac{a}{c} \delta_i \cos i = \frac{a}{c} \frac{I_A}{M_A a^2} \frac{P}{P_A} \sin\theta_A \cos i \quad (27)$$

if one can assume the orbital eccentricity is small. This effect, however, will be almost negligible in the case of PSR J0737-3039 because the inclination angle $i \simeq 90^\circ$.

For the advance of the periastron, the ratio of the spin-orbit and 1PN contributions is [24]

$$\begin{aligned} \frac{A_p}{A_{1PN}} &= -\frac{P}{6(1-e^2)^{1/2} M a^2} \sum_i \\ &\frac{I_i(4M_i + 3M_{-i})}{M_i P_i} (2\cos\theta_i + \cot i \sin\theta_i \sin\phi_i). \end{aligned} \quad (28)$$

In the case that $|\vec{S_A}| >> |\vec{S_B}|$, only the $i = A$ term contributes substantially. For comparison, both masses contribute to the 2PN contribution. In the case of equal masses, the periastron advance ratio of 2PN to 1PN is [24]

$$\frac{A_{2PN}}{A_{1PN}} = \frac{GM}{12ac^2} \left(\frac{189}{1-e^2} - 47 \right). \quad (29)$$

Assuming that the orientations of the spin of pulsar A can be eventually determined, which seems feasible given the large precessional amplitudes and the relatively short precession period, the accuracy of the determination of the moment of inertia rests upon determining the individual masses to sufficient accuracy. It is expected that within a few years a measurement of I_A to about 10% accuracy is feasible [25].

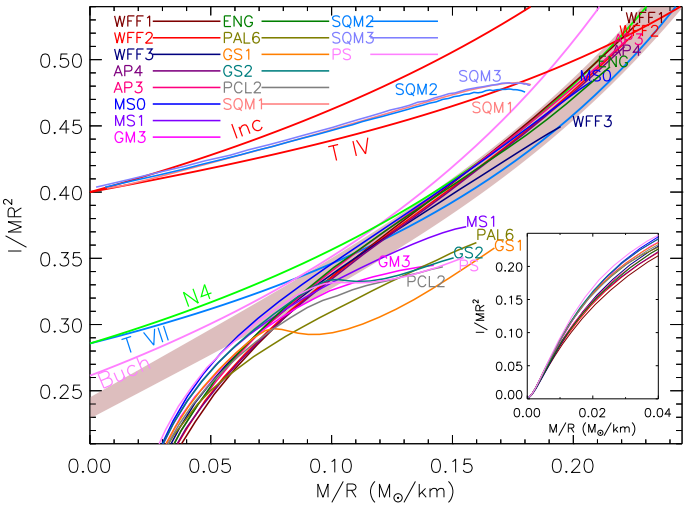

Figure 6: Moments of inertia are plotted versus M/R. Symbols for EOS's are taken from Ref. [1]. Analytic solutions are also plotted, including the constant density (Inc), Tolman (T IV) self-bound, Buchdahl (Buch), Tolman (T VII) and Nariai (N4) solutions discussed in the text. The shaded band is the fit described in Eq. 31. The inset shows the behaviors for $M/R \to 0$. Figure taken from Ref. [25].

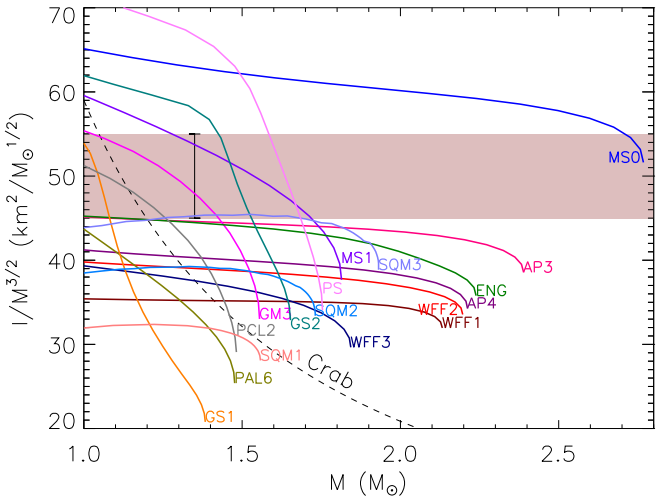

Figure 7: Moment of inertia scaled by $M^{3/2}$ versus M. The shaded band shows a hypothetical measurement of $I/M^{3/2} = 50 \pm 5$ km^2 M$_\odot^{-1/2}$. The error bar is set at the precise mass of $M_A = 1.34$ M$_\odot$. The dashed line 'Crab' is a lower limit derived in Ref. [26] for the Crab pulsar. Figure taken from Ref. [25].

The binary pulsar system PSR J0737-3039 consists of two neutron stars and has these physical parameters[22]:

$$\begin{aligned} \frac{GM}{ac^2} &= 4.32\ 10^{-6}, \quad P/P_A = 3.88\ 10^5, \\ \frac{I_A}{Ma^2} &= (7.74\ 10^{-11})\ I_{A,80}, \end{aligned} \tag{30}$$

where $I_{A,80} = I_A/(80\ \mathrm{M}_\odot\ \mathrm{km}^2)$. The moments of inertia for stars constructed with many of the normal matter equations of state used in Figures 2 and 3, together with those of some analytic solutions, are displayed in Figure 6. The shaded band shows a relatively EOS-independent relation among I, M and R

$$I \simeq (0.237 \pm 0.008)\ MR^2 \times \left[1 + 4.2\frac{M\ \mathrm{km}}{\mathrm{M}_\odot R} + 90\left(\frac{M\ \mathrm{km}}{\mathrm{M}_\odot R}\right)^4\right] \tag{31}$$

that describes normal neutron stars without significant low-density softening. Strange quark matter stars deviate substantially from this, however.

To remove the undetermined quantity R, Figure 7 shows the moment of inertia, scaled by $M^{3/2}$ to reduce the dynamic range, as a function of M. It seems clear that a measurement of I of the indicated precision could rule out many EOS's. Dimensionally, I scales with MR^2, so in principle a measurement of I with 10% accuracy implies an uncertainty in a radius estimate of about 5%, since M is known to much higher precision. The inferred value of R for a given measured pair $(I \pm 10\%, M \pm 0\%)$ is pictured by the shaded bands in Figure 8. Their widths contain the uncertainties inherent in the measurements of I and M and in Eq. 31. The single error bar shows the case $I_{A,80} = 1.0 \pm 0.1$ and $M_A = 1.34$ M$_\odot$.

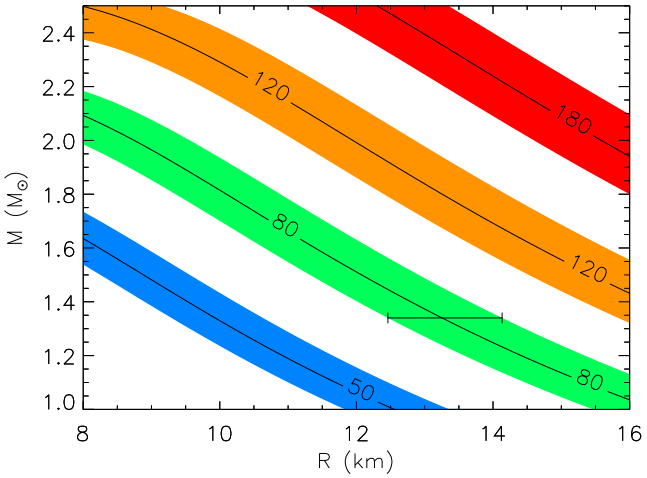

Figure 8: Bands show allowed regions for indicated hypothetical moment of inertia measurements with 10% uncertainty (units of M$_\odot$ km^2). The error bar is shows the case $I_{A,80} = 1.0 \pm 0.1$ and $M_A = 1.34$ M$_\odot$. Figure taken from Ref. [25].

6. RADIUS MEASUREMENTS

Most known neutron stars are observed as pulsars and have photon emissions from radio to X-ray wavelengths dominated by non-thermal emissions believed to be connected to the pulsar mechanism or the neutron star's magnetosphere. However, approximately a dozen isolated neutron stars with ages up to a million years old have been identified [27] with significant thermal emissions. Stars of these ages are are expected to have surface temperatures in the range of 3×10^5 K to 10^6 K, *i.e.,* they are predominately X-ray sources. If their total photon fluxes were that of a blackbody, they would obey

$$F_\infty = L_\infty/4\pi d^2 = \sigma T_\infty^4 (R_\infty/d)^2, \qquad (32)$$

where d is the distance, and T_∞, F_∞ and L_∞ refer to the temperature, flux and luminosity redshifted relative to their values at the neutron star surface. For example, $T_\infty = T/(1+z), F_\infty = F/(1+z)^2$. As a result, the radiation radius, $R_\infty = R(1+z)$, is a quantity that can be estimated if F_∞, T_∞ and d are known. R_∞ is a function of both M and R, but if redshift information is available, M and R could be uniquely determined. Contours of R_∞ are displayed in Fig. 2. A value of R_∞ requires both $R < R_\infty$ and

$$M < c^2 R_\infty/(3\sqrt{3}G) \simeq 0.13(R_\infty/\mathrm{km})\mathrm{M}_\odot. \qquad (33)$$

A serious problem in determining R_∞ and T_∞ is that the star's atmosphere rearranges the spectral distribution of emitted radiation, *i.e.,* they are not blackbodies [28]. Neutron star atmosphere models are mostly limited to non-magnetized atmospheres, although pulsars are thought to have intense mngnetic fields $\geq 10^{12}$ G. Strongly magnetized hydrogen is relatively simple, but magnetized heavy element atmospheres are still in a state of infancy.

A few cases exist in which the neutron star is sufficiently close for detection of optical radiation. These stars are observed to have optical fluxes factors of 3–5 times greater than a naive blackbody extrapolation from the X-ray range would imply. This optical excess is a natural consequence of the neutron star atmosphere, and results in an inferred R_∞ substantially greater than that deduced from the X-ray blackbody alone. In many cases a heavy-element atmosphere appears to fit the global spectral distributions from X-ray to optical energies while also yielding neutron star radii in a plausible range. However, the observed absence of narrow spectral features, predicted by heavy-element atmosphere models, is puzzling [29]. Perhaps severe broadening of spectral features is caused by intense magnetic fields or high pressures. Another possibility is that intense magnetic fields produce a phase transition in which the atmosphere disappears, and a bare heavy-element surface is exposed.

The estimation of radii from isolated neutron stars is also hampered by uncertainties of source distance. Distances to pulsars can be estimated by their dispersion measures to factors of 2 or 3, but in a few cases parallax distances are possible. Parallaxes of three sources (Geminga, RX J185635-3754 and PSR B0656+14) have been obtained [30], but errors are still large. As a consequence, values of R_∞ determined from thermally-emitting neutron stars, while in a plausible range, are not sufficiently precise at present to usefully restrict properties of dense matter.

In this context, the recent discovery of thermal radiation from quiescent X-ray bursters in globular clusters is particularly interesting [31]. These systems contain rejuvenated billions of years-old neutron stars heated by recent episodes of mass accretion from their companions. Since the accreted material is dominated by hydrogen, and accretion is believed to quench magnetic fields, these stars may have the simplest of all possible atmospheres: non-magnetic hydrogen. Current results are consistent with radiation radii $R_\infty \sim 12$ km, but accuracies are limited by systematic uncertainties in the intervening interstellar hydrogen column density, since this material obscures 50% or more of the X-ray flux. Interestingly, the distances to these sources will likely become relatively well known in the near future, reducing a source of error that plagues interpretations of isloated neutron stars.

Acknowledgments

I wish to thank my coworkers M. Prakash, A. Steiner, D. Page and B. Schutz for many influential discussions and suggestions. Much of the material presented here is from joint publications. I also wish to add a personal note of appreciation on behalf of P.J. Ellis, who passed away in February 2005, for many pleasurable years of collaboration and friendship.

Work supported by Department of Energy contract DE-FG03-87ER40317.

References

[1] J.M. Lattimer & M. Prakash, Astrophys. J. 550 (2001) 426.
[2] J.M. Lattimer, M. Prakash, D. Masak & A. Yahil, Astrophys. J. 355 (1990) 241.
[3] N.K. Glendenning, Phys. Rev. D 46 (1992) 1274.
[4] B. Link, R.I. Epstein & J.M. Lattimer, Phys. Rev. Lett. 83 (1999) 3362.
[5] J.M. Lattimer & M. Prakash, Science 304 (2004) 536.

[6] J.P. Blaizot, J.F. Berger, J. Dechargé & M Girod, Nucl. Phys. A591 (1995) 431; D. H. Youngblood, H.L. Clark & Y.-W. Lui, Phys. Rev. Lett. 82 (2999) 691.
[7] J.M. Pearson, Phys. Lett. B271 (1991) 12; S. Rudac, P.J. Ellis, E.K. Heide & M. Prakash, Phys. Lett. B285 (1992) 183.
[8] P. Danielewicz, Nucl. Phys. A 727 (2003) 233.
[9] A.W. Steiner, M. Prakash, J.M. Lattimer & P.J. Ellis, Phys. Rep. (2005), in press; astro-ph/0410066.
[10] R.C. Tolman, Phys. Rev. 55 (1939) 364.
[11] H. Nariai, Sci. Rep. Tohoku Univ. Ser. 1 34 (1950) 160; 35 (1951) 62.
[12] H.A. Buchdahl, Astrophys. J. 147 (1967) 310.
[13] K. Lake, Phys. Rev. D67 (2003) 104015.
[14] J.M. Lattimer & M. Prakash, Phys. Rev. Lett. (2005), in press; astro-ph/0411280.
[15] C.E. Rhoades & R. Ruffini, Phys. Rev. Lett. 32 (1974) 324.
[16] R.N. Manchester, Science 304 (2004) 542.
[17] J.M. Weisberg & J.H. Taylor, in Binary Radio Pulsars, eds. F.A. Rasio and I.H. Stairs (Ast. Soc. Pac., San Francisco, 2004).
[18] H.A. Bethe & Brown, Astrophys. J. 506 (1998) 780.
[19] H. Quaintrell, A.J. Norton, T.D.G. Ash, P. Roche, B. Willetus, T.R. Bedding, I.K. Baldry & R.P. Fender, Astron. Astrophys. 401 (2003) 303.
[20] J.S. Clark, S.P. Goodwin, P.A. Crowther, L. Kaper, M. Fairbairn, N. Langer & C. Brocksopp, Astron. Astrophys. 392 (2002) 909.
[21] P.G. Jonker, D. Steeghs, G. Nelemans and M. van der Klis, Mon. Not. Roy. Ast. Soc. 356 (2005) 621.
[22] A.G. Lyne, M. Burgay, M. Kramer, A. Possenti, R.N. Manchester, F. Camilo, M.A. McLaughlin, D.R. Lorimer, N. D'Amico, B.C. Joshi, J. Reynolds & P.C.C. Freire, Science 303 (2004) 1153.
[23] B.M. Barker & R.F. O'Connell, Phys. Rev. D12 (1975) 329.
[24] T. Damour & G. Schaefer, Nuovo Cimento 101B (1988) 127.
[25] J.M. Lattimer & B.F. Schutz, Astrophys. J. (2005), in press; astro-ph/0411470.
[26] M. Bejger & P. Haensel, Astron. Astrophys. 405 (2003) 747.
[27] D. Page, J. M. Lattimer, M. Prakash & A. W. Steiner, Astrophys. J. Supp. 155 (2004) 623.
[28] R. Romani, Astrophys. J. 313 (1987) 718.
[29] V. Burwitz, V. E. Zavlin, R. Neuhäuser, P. Predehl, J. Trümper, & A. C. Brinkman, Astron. Astrophys. 379 (2001) L35.
[30] F. M. Walter & J.M. Lattimer, Astrophys. J. 576 (2002) L145.
[31] R.E. Rutledge, L. Bildsten, E.F. Brown, G.G. Pavlov, V.E. Zavlin G. Ushomirsky, Astrophys. J. 580 (2002) 413; R.E. Rutledge, L. Bildsten, E.F. Brown, G.G. Pavlov & V.E. Zavlin, Astrophys. J. 514 (1999) 945; 529 (2000) 985; 551 (2001) 921; 559 (2001) 1054; C.O. Heinke, J.E. Grindlay, D.A. Lloyd & P.D. Edmonds. Astrophys.J. 588 (2003) 452.